The Journal of Neuroscience

November 14, 2007 • Volume 27 Number 46 • www.jneurosci.org

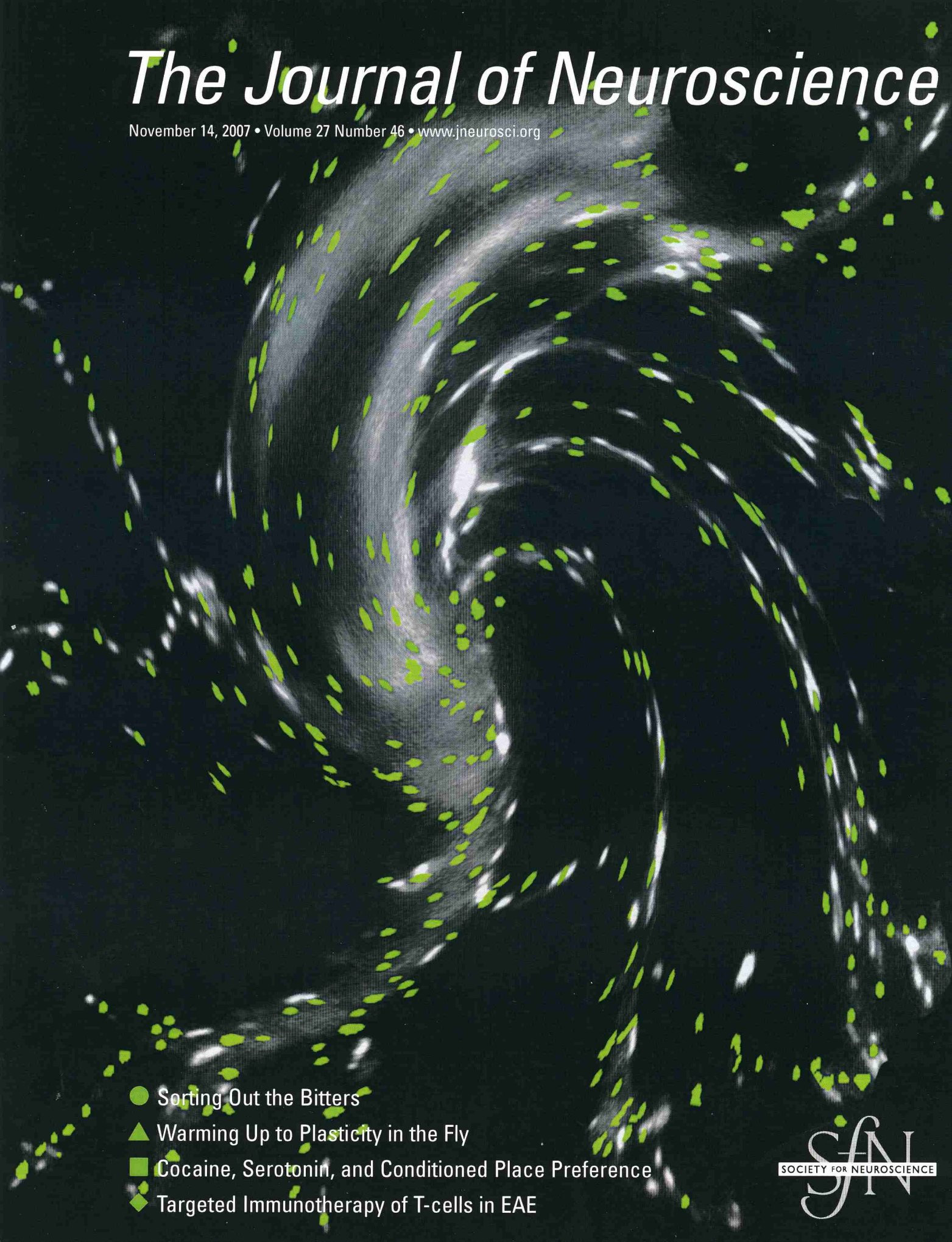

- Sorting Out the Bitters
- Warming Up to Plasticity in the Fly
- Cocaine, Serotonin, and Conditioned Place Preference
- Targeted Immunotherapy of T-cells in EAE

SFN SOCIETY FOR NEUROSCIENCE

Toolbox

Editor's Note: Toolboxes are intended to briefly highlight a new method or a resource of general use in neuroscience or to critically analyze existing approaches or methods. For more information, see http://www.jneurosci.org/misc/itoa.shtml.

Surface Trafficking of Neurotransmitter Receptor: Comparison between Single-Molecule/Quantum Dot Strategies

Laurent Groc,[1] Mathieu Lafourcade,[1] Martin Heine,[1] Marianne Renner,[1] Victor Racine,[3] Jean-Baptiste Sibarita,[3] Brahim Lounis,[2] Daniel Choquet,[1] and Laurent Cognet[2]

[1]Physiologie Cellulaire de la Synapse, Unité Mixte de Recherche (UMR) 5091, Centre National de la Recherche Scientifique (CNRS), Université Bordeaux 2, 33077 Bordeaux, France, [2]Centre de Physique Moléculaire Optique et Hertzienne, UMR 5798, CNRS, Université Bordeaux 1, 33405 Talence, France, and [3]Curie Institute, Research Division, UMR 144-CNRS, 75005 Paris, France

The cellular traffic of neurotransmitter receptors has captured a lot of attention over the last decade, mostly because synaptic receptor number is adjusted during synaptic development and plasticity. Although each neurotransmitter receptor family has its own trafficking characteristics, two main modes of receptor delivery to the synapse have emerged: endo-exocytotic cycling and surface diffusion [e.g., for glutamatergic receptors, see Bredt and Nicoll (2003) and Groc and Choquet (2006)]. Receptor cycling through endo-exocytotic processes can be measured by several experimental means, from biochemical to imaging assays. The use of fluorescent protein (XFP)-tag imaging provides a powerful approach to investigate the trafficking of receptor clusters between neuronal compartments (e.g., soma, dendrite, spine) (Kennedy and Ehlers, 2006). A disadvantage of the XFP-tag approach in live experiment is extreme difficulty in detecting XFP fluorescence signals from small nonclustered receptor pool (Cognet et al., 2002; Lippincott-Schwartz and Patterson, 2003). XFP-tagged neurotransmitter receptors are often present in several cellular compartments from the endoplasmic reticulum to the plasma membrane with various relative contents. For instance, surface XFP-tagged neurotransmitter receptors represent only a minor fraction of the total receptor population, precluding their specific detection. Alternative live-cell imaging approaches were thus required to specifically isolate surface receptors. Interestingly, a variant of the green fluorescent protein (GFP), ecliptic pHluorin, shows a reversible excitation ratio change between pH 7.5 and 5.5, and its absorbance decreases as the pH is lowered. Most neurotransmitter receptors, including the ionotropic glutamate ones, display an extracellular N-terminal region, implying that the N terminus will always be in an acidic environment inside the cell, whereas it will be exposed to a neutral pH after insertion into the plasma membrane. By this means, surface receptors can be specifically detected and tracked with live-imaging approaches (Ashby et al., 2004). Alternatively, surface receptors can be labeled and detected by immunocytochemical approaches using antibodies directed against receptor extracellular epitopes.

The purpose of this Toolbox is to outline currently available approaches to measure the surface trafficking of receptor in neurons, with a special emphasis on single-molecule (organic dye) and quantum dot (QDot) detection for neurotransmitter receptor tracking.

Exploring receptor surface trafficking: approaches

Investigation of receptor surface distribution and diffusion can be sorted in two groups. On the one hand, the average surface diffusion of labeled receptors is studied without distinction of individual behaviors (Fig. 1*A*). Surface receptors can be isolated by electrophysiologically tagged methods (Tovar and Westbrook, 2002; Adesnik et al., 2005; Thomas et al., 2005). Schematically, a subpopulation of surface receptors is irreversibly blocked (e.g., MK-801 for NMDA receptors) and the receptor surface diffusion is estimated from time-dependent functional recovery after receptor blockade. Another approach is based on the fluorescence labeling techniques coupled to live fluorescence microscopy, such as fluorescent recovery after photobleaching (FRAP) of pHluorin-tagged receptors (Rasse et al., 2005; Ashby et al., 2006; Kopec et al., 2006; Lober et al., 2006; Sharma et al., 2006). Note that both

Received April 11, 2007; revised Sept. 18, 2007; accepted Oct. 2, 2007.

This work was supported by grants from the Centre National de la Recherche Scientifique, Conseil Régional d'Aquitaine, Ministère de la Recherche, and Fondation pour la Recherche Médicale and by a European Community Grant (GRIPANT, CT-2005-005320). We thank Richard Huganir for the cDNA BGG construct and Christelle Breillat, Beatrice Teissier, and Delphine Bouchet for technical assistance.

Correspondence should be addressed to Laurent Groc, Unité Mixte de Recherche 5091, Centre National de la Recherche Scientifique, Université Bordeaux 2, 146 rue Léo Saignat, 33077 Bordeaux, France. E-mail: laurent.groc@u-bordeaux2.fr.

DOI:10.1523/JNEUROSCI.3349-07.2007

 0270-6474/07/2712433-05$15.00/0

approaches provided equivalent characteristics of receptor surface diffusion [e.g., for AMPA receptor in hippocampal cultured neurons (Adesnik et al., 2005; Ashby et al., 2006)], indicating that ensemble surface receptor diffusion can efficiently be measured using either approaches.

Opposite to the ensemble methods, single-molecule detection methods retrieve the diffusion properties of individual labeled receptors over time (Fig. 1*A*). The typical outcome is the complete distribution of the behavior of surface neurotransmitter receptors, which have revealed non-Gaussian shapes and a variety of diffusion characteristics at a given time. To date, this approach has unraveled the surface trafficking of neurotransmitter receptors and channels, including glutamatergic metabotropic mGluR5, AMPA and NMDA receptors (Borgdorff and Choquet, 2002; Serge et al., 2002; Tardin et al., 2003; Groc et al., 2004; Howarth et al., 2005; Groc et al., 2006), glycine (Meier et al., 2001; Dahan et al., 2003), GABA receptors (Bouzigues and Dahan, 2007), and Kv potassium channels (O'Connell et al., 2006). To label single molecules, there are essentially two possibilities: the use of a single dye (SD) or a single particle (SP) (e.g., nano-sized QDots). The SD tags are short lived but small size, whereas SP tags allow long observation times, but the size of the label can prevent its access to specific confined cellular areas.

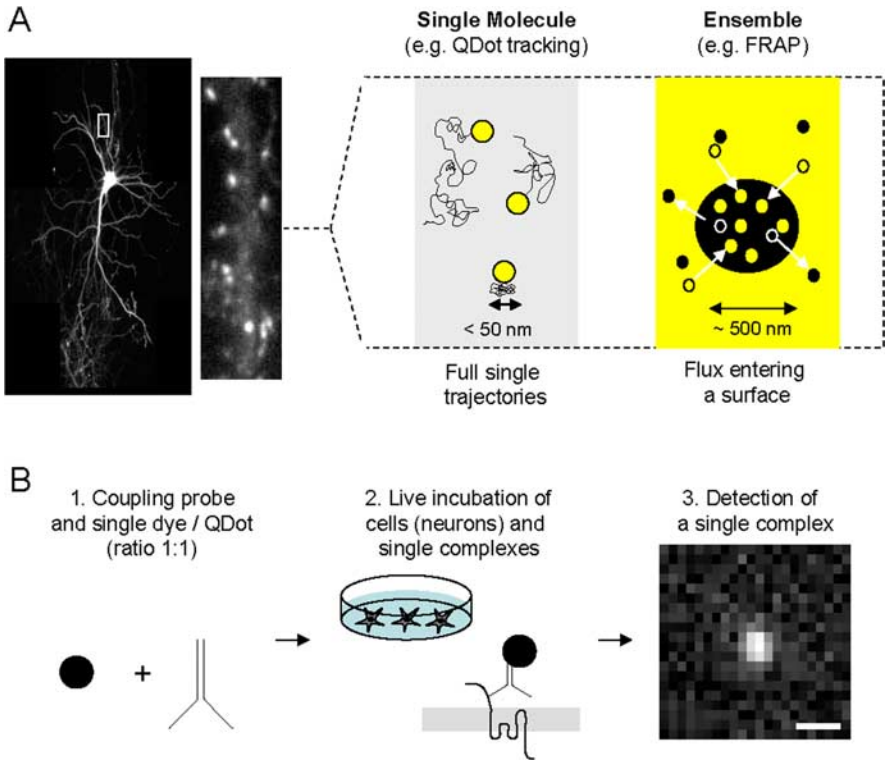

Figure 1. Schematic description of single-molecule/particle experiment for the tracking of surface receptors in neurons. ***A***, The first choice to make when planning to study receptors at the surface of neurons (left, hippocampal neuron expressing GFP-Homer 1C) is the type of experimental approach to setup. Right, There are schematically two ways to examine surface trafficking of receptors: ensemble or single-molecule approaches. The first one measures the surface behavior of the ensemble of labeled receptors using, for instance, FRAP. The second one measures the surface behavior of one (or possibly two if using antibody) receptor using single-molecule or Dot tracking. Although both approaches provide good measurements of receptor surface diffusion, differences in time and spatial resolutions exist. For instance, the spatial resolution in the type of microscopy used for FRAP and Dot experiments is defined by the diffraction limit, typically on the order of 200–300 nm. The single-molecule technique provides, however, a 10 nm pointing accuracy, which provides a unique way to collect the number of points necessary to build a trajectory in submicrometer membrane domains (e.g., synapse, lipid raft). ***B***, Experimental procedure to run single-molecule or Dot tracking. First, the label used to detect the molecule of interest (e.g., antibody) is coupled to the tag (single dye, single Dot) in the ratio 1:1 (left). Second, live neurons are incubated with the single tag complexes (high dilution, ~1 ng/ml) for several minutes. Third, single tag complexes are detected and tracked (see Single dye tracking and QDot tracking) over time as exemplified by the detection of a single Dot on a 30 ms acquisition image using a CCD camera. Scale bar, 600 nm. To ensure that the tracked complexes are in majority at the surface, rates of endocytosis of the receptor of interest should be first measured. SDT can then be performed during a time window in which only a low percentage (classically set as <15–20%) of receptors are internalized. For example, AMPAR surface tracking is performed only during 20 min after labeling, ensuring that <10–20% of labeled receptors are internalized. Note that the newly internalized AMPARs are mostly immobile and represent a small fraction of the single-molecule signals (Tardin et al., 2003).

Single dye tracking

SD tracking (SDT) first requires the attachment of a single tag (e.g., organic dye) to the molecular target through a specific high-affinity ligand that recognizes the extracellular domain of the molecular target in live cells (Fig. 1*B*). Labeling must be performed at low tag densities to be optically resolved (typically <1 molecule/μm^3) and to avoid cross-linking in the case of multivalent ligands (e.g., antibody). The second obvious requirement is to obtain signals from an SD that are large enough to overcome both the background noise from the molecule environment and that of the detection system (Fig. 1*B*). Several dyes fulfill these requirements, such as cyanine dyes (Cy3 or Cy5) that can be detected with good signal-to-noise ratios in live cells. The main limitation of SDT is, however, photobleaching, i.e., the processes by which photochemical reactions transform the excited fluorophore into a nonfluorescent product. It limits imaging time of a SD to typically a few seconds. Note that the use of antioxidant, such as Trolox, provides an efficient way to significantly reduce photobleaching and thus improve photostability (Rasnik et al., 2006).

In practice, single molecules are identified by their diffraction-limited signals, their well defined intensities, and the one-step photobleaching behavior (supplemental Box 1, available at www.jneurosci.org as supplemental material). Two-dimensional fitting by a Gaussian approximating the true point spread function of the microscope allows sub-wavelength localization of the labels (Cheezum et al., 2001), typically <50 nm for SDs in live cells (Tardin et al., 2003). Finally, once SDs are identified in each image frame, their two-dimensional trajectories can be constructed using a Vogel algorithm. This algorithm performs a correlation analysis between the positions of the SD found in consecutive images (Schmidt et al., 1995) (supplemental Box 2, available at www.jneurosci.org as supplemental material).

QDot tracking

QDots are passivated semiconductor nanocrystals that are water soluble and functionalized for biological applications. In addition to their superior brightness compared with SD, QDots have a larger absorption cross section, such that they can be excited with a mercury lamp. This allows recording large fields of view and

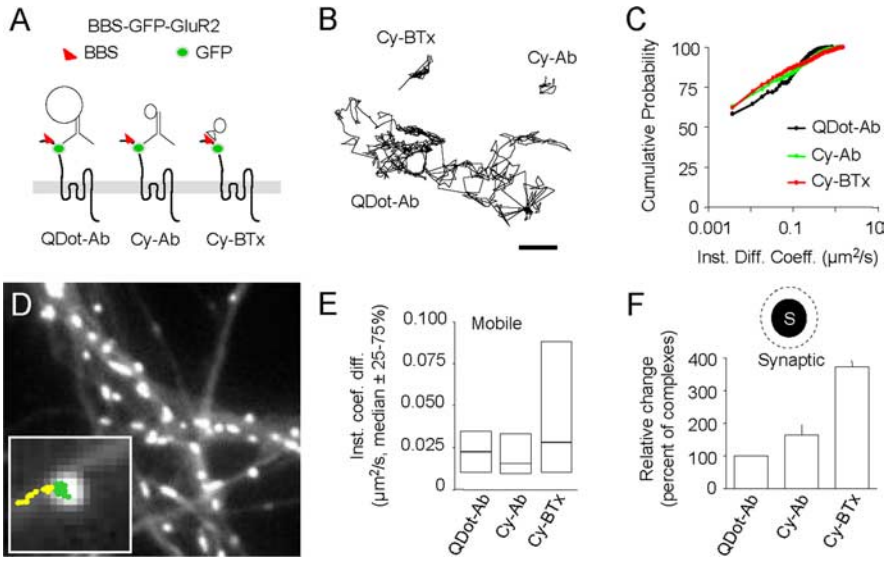

Figure 2. Tracking of a BBS-GFP-tagged GluR2 subunit using three different single-molecule/particle approaches. ***A***, Schematic representation of the BGG and the single-molecule/particle complexes: Dot coupled to antibody directed against GFP (left), cyanine 5 coupled to an antibody directed against GFP (center), and cyanine 5 coupled to bungarotoxin (right). The insertion of the BGG into the surface membrane was observed by incubating neurons transfected with BGG with bungarotoxin coupled to Alexa 568 (data not shown). Hippocampal neurons from 18-d-old rat embryos were cultured on glass coverslips following the Banker technique. For BGG expression, hippocampal neurons cultured 8–11 d *in vitro* were transfected with 1 μg of BGG cDNA for 24–36 h before the experiment using Lipofectamine 2000 reagent. Surface BGGs were detected by immunocytochemistry after live incubation with Alexa568-bungarotoxin (data not shown). Because cultured neurons can express low levels of endogenous nicotinic acetylcholine receptors, neurons were incubated with the nicotinergic receptor antagonist methyllycaconitine (10 nM, 20 min, 37°C) during single tag tracking. Finally, for single-molecule tracking, cyanine 3 or cyanine 5 was coupled to bungarotoxin or to the rabbit polyclonal anti-GFP antibody. For quantum dot (QD) tracking, QD 655 goat F(Ab')2 anti-rabbit IgGs (0.1 μM) were coupled with the polyclonal antibodies against GFP (1 μg). ***B***, Representative extrasynaptic trajectories from the three different surface single-molecule/particle complexes. Scale bar, 600 nm. Note the difference in trajectory length as a result of the photostability of single Dot when compared with cyanine 5 fluorophores. ***C***, Cumulative distributions of the instantaneous diffusion coefficient (bin size = 0.075 $\mu m^2/s$) ($p > 0.05$ for all comparisons, Kolmogorov–Smirnov test). The median values were not significantly different (QDot-Ab = 1×10^{-3} $\mu m^2/s$, IQR = 0–0.049 $\mu m^2/s$, $n = 1498$ trajectories; Cy-Ab = 2×10^{-3} $\mu m^2/s$, IQR = 1×10^{-4}–0.049 $\mu m^2/s$, $n = 919$; Cy-BTx = 4×10^{-3} $\mu m^2/s$, IQR = 0–0.025 $\mu m^2/s$, $n = 1387$; $p > 0.05$, Mann–Whitney *U* test). The percentage of immobile receptor (first point of the cumulative distribution) and the instantaneous diffusion coefficient (Inst. Diff. Coeff.) of the mobile molecules/particles (set to $D > 0.0075$ $\mu m^2/s$) were also not significantly different between complexes. All trajectories (each condition) were obtained from 30–60 dendritic fields and three to five different culture preparations. ***D***, Labeling of synapses using Mitotracker (1 min at 1 nM). Synaptic trajectories (green) are defined by their colocalization with synaptic labeling, the trajectory outside synapse being considered as extrasynaptic (yellow). Note the change in surface diffusion from a free diffusion behavior (extrasynaptic, yellow) to a confined one (synaptic, green). ***E***, Comparison of the instantaneous diffusion coefficient of mobile molecules/particles ($p < 0.05$, Mann-Whitney *U* test between Cy-BTx and the two other complexes). Note the subset of highly diffusing receptor detected with Cy-BTx. However, the instantaneous diffusion coefficient of all trajectories (QDot-Ab = 5×10^{-3} $\mu m^2/s$, IQR = 4×10^{-4}–0.023 $\mu m^2/s$, $n = 45$; Cy-Ab = 5×10^{-3} $\mu m^2/s$, IQR = 0–0.024 $\mu m^2/s$, $n = 98$; Cy-BTx = 10×10^{-3} $\mu m^2/s$, IQR = 7×10^{-4}–0.035 $\mu m^2/s$, $n = 51$; $p > 0.05$, Kruskal–Wallis test) and the percentage of immobile receptors ($p > 0.05$) were not significantly different between complexes. ***F***, Percentage of dyes/QDots detected within the synapse (QDot-Ab = 5.4 ± 1.3%, $n = 9$ dendritic areas; Cy-Ab = 9.4 ± 2.3%, $n = 33$; Cy-BTx = 20.3 ± 5.2%, $n = 35$; $p < 0.01$, ANOVA followed by Tukey's *post hoc* test). Note the relative increase toward smaller complexes.

gaining parallelism in data acquisition. Importantly, QDots are much more photostable than SDs, although they are subject to blinking (Michalet et al., 2005). However, these nanoparticles are still bigger than organic dyes and rather bulky (~10–30 nm).

Because of the larger signals obtained from QDots than from SDs, a faster detection algorithm than the two-dimensional Gaussian fitting of the luminescent signal was developed. It relies on wavelet transforms that filter the image frames and identify the QDots through their morphology and not their intensity. This algorithm provides minimal time and memory consumption and provides clear advantages when recording large images and very long QDot-based trajectories (supplemental Box 2, available at www.jneurosci.org as supplemental material). To account for the blinking of luminescent QDots, an algorithm was further used to reconnect iteratively portions of trajectories originating from the same QDots. The parameters of reconnection (maximum distance between reconnected events and maximum "dark" time) are adjusted according to the diffusion time of the molecules and the image acquisition rate. To prevent false reconnections, the surface density of QDots must be low enough that parameters of reconnection can be found without mixing the trajectories of different QDots. In practice, the maximum distance of reconnection is on the order of the mean QDot image-to-image steps and at least 10 times smaller than the mean distance between different QDots. It should be mentioned that other analytical approaches have been developed to overcome the problem of QDot blinking in trajectory reconstructions (Bonneau et al., 2005; Bachir et al., 2006). Interestingly, QDot blinking provides a criterion to identify individual QDots, because fluorescence changes between "on" and "off" states for a single Dot alternate only in two levels.

Does the size and valence of single tag complexes influence surface diffusion?

At the scale of the nano-sized probes, movements of surface extrasynaptic receptors are not governed by the mass of the probe, but instead by the motion of the membrane protein. Indeed, the viscosity of membranes is 100- to 1000-fold greater than that of extracellular medium. In restricted environments, however, like in the synaptic cleft, the size and valence of a single complex can impact surface receptor diffusion. The impact of different labeling strategies on SD/QDot measurements in nonconfined cellular environments (the extrasynaptic membrane) and confined ones (synapses labeled with Mitotracker) (Tardin et al., 2003; Groc et al., 2004) was measured. Cultured hippocampal neurons were transfected with the GluR2 AMPA receptor subunit tagged with a bungarotoxin binding site (BBS; 13 aa) and a GFP on an extracellular loop (Sekine-Aizawa and Huganir, 2004). The BBS-GFP-tagged GluR2 (BGG) subunits were then tracked at the neuronal surface using three different single-molecule complexes that have different sizes (QDot-Ab > Cy5-Ab > Cy5-BTx) and valences (QDot-Ab/Cy5-Ab/Cy5-BTx: 2/2/1), where QDot-Ab stands for QDots coupled to anti-GFP antibody (Ab, ~150 kDa); Cy5-Ab for a cyanine 5 (Cy5) coupled to anti-GFP antibody; and Cy5-BTx for a Cy5 coupled to bungarotoxin (BTx, 8 kDa) (Fig. 2*A*). The comparison of the diffusion of the three complexes in the extrasynaptic membrane revealed that the cumulative distributions of instantaneous

diffusion coefficients (Fig. 2*B*,*C*) and the median values of the total and mobile receptors were not significantly different.

Within synapses (Fig. 2*D*), the median values of instantaneous diffusion coefficients for all trajectories were also not significantly different, and neither were the percentage of immobile receptors (Fig. 2*E*). Interestingly, the distributions of the instantaneous diffusion coefficient for the only mobile receptors were different: Cy5-BTx complexes displayed a broader range than QDot-Ab and Cy5-Ab (Fig. 2*E*). Consistently, the median value of the Cy5-BTx distribution was significantly higher than the one of QDot-Ab and Cy5-Ab. Together, these results indicate that the three antibody-based complexes provide an equivalent picture of the proportion of diffusing synaptic receptors, although the smaller complex allow the additional visualization of a subset of highly diffusing receptors.

Regarding receptor diffusion within synaptic areas, two points should be discussed. First, synapses could be labeled using various markers, either presynaptic (e.g., Mitotracker, synaptotagmin) or postsynaptic (e.g., PSD-95, Homer 1c) (Tardin et al., 2003; Groc et al., 2004; Bats et al., 2007; Ehlers et al., 2007) (Figs. 1, 2). Comparing diffusion of AMPA receptors within synapses labeled with either Mitotracker (presynaptic) or Homer 1c (postsynaptic) shows almost similar diffusion characteristics (indistinguishable percentage of immobile receptors and exchange rate between extrasynaptic and synaptic membrane but a slight difference in the diffusion constant) (our unpublished data). Second, Dot functionalizing strategies can influence synaptic diffusion likely through difference in size and steric properties. For instance, diffusion distributions of synaptic GluR2 subunit are slower when measured with QDots coated with protein A (~50 kDa) [median = 0.005 $\mu m^2/s$, interquartile range (IQR; 25–75%) = 0.0005–0.03, $n = 59$] (Groc et al., 2004) compared with QDots coated with Fab fragment (20 kDa) (QDot-Fab: median = 0.025 $\mu m^2/s$, IQR = 0.0012–0.11, $n = 366$). In conclusion, all examined probes allow the tracking of synaptic receptors, but it appears that the smaller the probe, the better the tracking of fast diffusing synaptic receptors. This further encourages the development of very small probes (only few nanometers) for confined environments.

Do the different single-tagged complexes penetrate equally the synaptic cleft?

To answer this question, surface tag complexes were counted for each image series and were affected as extrasynaptic, synaptic, or juxtasynaptic (300–500 nm around the labeled synapses). In total, 150,584 molecules/particles were analyzed. The percentage of tag complexes localized within synapses (synaptic over total molecule number) averaged ~20% (range 0–26%). Interestingly, the synaptic content of Cy5-Ab and Cy5-BTx molecules was higher than that of QDot-Ab (Fig. 2*F*). However, in the juxtasynaptic membrane, this difference vanished, indicating that the size of single complexes is likely to affect the accessibility of the complexes to the highly confined synaptic cleft.

Are surface diffusions of endogenous and transfected receptor similar?

Recombinant receptor subunits are, and will be, widely used to study receptor trafficking during various paradigms of neuronal function. The simple but important question of whether endogenous and transfected receptors behave similarly at the neuronal surface appeared. The surface diffusion of both endogenous and transfected recombinant glutamatergic subunits were then compared using data collected from published (Groc et al., 2006; Bats et al., 2007) and unpublished (supplemental Box 3, available at www.jneurosci.org as supplemental material) studies. It emerged that overexpressed GluR or NR glutamatergic subunits exhibit either similar or different surface trafficking, respectively, when compared with endogenous ones. These results are only indicative for specific experimental designs and may vary with different transfection method, subunit types, or neuronal stages. Such comparison strongly suggests that pertinent controls (e.g., comparison between endogenous and recombinant subunit surface trafficking) should automatically be performed.

Future directions

What are the "ideal" probes for future single-molecule/particle tracking? The obvious and straightforward answer is to develop probes that are as small as possible, photoresistant, and with very limited blinking. Although the QDots are photoresistant and exhibit blinking, their actual multilayer water-stabilizing structure and coupling with antibodies (or streptavidin) results in tens-of-nanometers-size Dot complexes that equal the size of the synaptic cleft (results above). The engineering of smaller QDots, directly coupled to the detection probes (e.g., antibody or synthetic peptide), will surely improve the Dot-based complexes (Pinaud et al., 2004; Michalet et al., 2005). The tracking of individual few-nanometer gold particles in live neurons using a photothermal technique offers a promising alternative because it has the unique potential to record long trajectories (no theoretical limit) from very small probes (5 nm wide) (Lasne et al., 2006). As for the ligands, the engineering of small probes ($\ll$antibody or streptavidin) with high affinity will offer alternative ways, although the effects of recombinant subunit overexpression on cellular trafficking have to be carefully assayed. Finally, one aim of the cellular neuroscience field is to track receptors directly from live brains. Current roadblocks of this approach are based on *in vivo* imaging (multiphoton microscopy) of XFP-tag receptors in neurons that have been previously infected by virus (e.g., Sindbis virus, lentivirus) containing the XFP-tag receptor constructs (Svoboda and Yasuda, 2006). Whether pHluorin-XFP for ensemble measurements or QDots, organic molecules, and nanogold particles for single particle approaches will be the appropriate probes for receptor surface tracking *in vivo* remains an open and exciting question.

References

Adesnik H, Nicoll RA, England PM (2005) Photoinactivation of native AMPA receptors reveals their real-time trafficking. Neuron 48:977–985.

Ashby MC, Ibaraki K, Henley JM (2004) It's green outside: tracking cell surface proteins with pH-sensitive GFP. Trends Neurosci 27:257–261.

Ashby MC, Maier SR, Nishimune A, Henley JM (2006) Lateral diffusion drives constitutive exchange of AMPA receptors at dendritic spines and is regulated by spine morphology. J Neurosci 26:7046–7055.

Bachir A, Durisic N, Grutter P, Wiseman P (2006) Characterization of blinking dynamics in quantum dot ensembles using image correlation spectroscopy. J Appl Phys 99:064503.

Bats C, Groc L, Choquet D (2007) The interaction between Stargazin and PSD-95 regulates AMPA receptor surface trafficking. Neuron 53:719–734.

Bonneau S, Dahan M, Cohen L (2005) Single quantum dot tracking based on perceptual grouping using minimal paths in a spatiotemporal volume. IEEE Trans Image Process 14:1384–1395.

Borgdorff AJ, Choquet D (2002) Regulation of AMPA receptor lateral movements. Nature 417:649–653.

Bouzigues C, Dahan M (2007) Transient di-

rected motions of GABA(A) receptors in growth cones detected by a speed correlation index. Biophys J 92:654–660.

Bredt DS, Nicoll RA (2003) AMPA receptor trafficking at excitatory synapses. Neuron 40:361–379.

Cheezum M, Walker W, Guilford W (2001) Quantitative comparison of algorithms for tracking single fluorescent particles. Biophys J 81:2378–2388.

Cognet L, Coussen F, Choquet D, Lounis B (2002) Fluorescence microscopy of single autofluorescent proteins for cellular biology. C R Acad Sci IV 3:645–656.

Dahan M, Levi S, Luccardini C, Rostaing P, Riveau B, Triller A (2003) Diffusion dynamics of glycine receptors revealed by single-quantum dot tracking. Science 302:442–445.

Ehlers MD, Heine M, Groc L, Lee MC, Choquet D (2007) Diffusional trapping of GluR1 AMPA receptors by input-specific synaptic activity. Neuron 54:447–460.

Groc L, Choquet D (2006) AMPA and NMDA glutamate receptor trafficking: multiple roads for reaching and leaving the synapse. Cell Tissue Res 326:423–438.

Groc L, Heine M, Cognet L, Brickley K, Stephenson FA, Lounis B, Choquet D (2004) Differential activity-dependent regulation of the lateral mobilities of AMPA and NMDA receptors. Nat Neurosci 7:695–696.

Groc L, Heine M, Cousins SL, Stephenson FA, Lounis B, Cognet L, Choquet D (2006) NMDA receptor surface mobility depends on NR2A–2B subunits. Proc Natl Acad Sci USA 103:18769–18774.

Howarth M, Takao K, Hayashi Y, Ting AY (2005) Targeting quantum dots to surface proteins in living cells with biotin ligase. Proc Natl Acad Sci USA 102:7583–7588.

Kennedy MJ, Ehlers MD (2006) Organelles and trafficking machinery for postsynaptic plasticity. Annu Rev Neurosci 29:325–362.

Kopec CD, Li B, Wei W, Boehm J, Malinow R (2006) Glutamate receptor exocytosis and spine enlargement during chemically induced long-term potentiation. J Neurosci 26:2000–2009.

Lasne D, Blab GA, Berciaud S, Heine M, Groc L, Choquet D, Cognet L, Lounis B (2006) Single nanoparticle photothermal tracking (SNaPT) of 5-nm gold beads in live cells. Biophys J 91:4598–4604.

Lippincott-Schwartz J, Patterson GH (2003) Development and use of fluorescent protein markers in living cells. Science 300:87–91.

Lober RM, Pereira MA, Lambert NA (2006) Rapid activation of inwardly rectifying potassium channels by immobile G-protein-coupled receptors. J Neurosci 26:12602–12608.

Meier J, Vannier C, Serge A, Triller A, Choquet D (2001) Fast and reversible trapping of surface glycine receptors by gephyrin. Nat Neurosci 4:253–260.

Michalet X, Pinaud FF, Bentolila LA, Tsay JM, Doose S, Li JJ, Sundaresan G, Wu AM, Gambhir SS, Weiss S (2005) Quantum dots for live cells, in vivo imaging, and diagnostics. Science 307:538–544.

O'Connell KMS, Rolig AS, Whitesell JD, Tamkun MM (2006) Kv2.1 potassium channels are retained within dynamic cell surface microdomains that are defined by a perimeter fence. J Neurosci 26:9609–9618.

Pinaud F, King D, Moore HP, Weiss S (2004) Bioactivation and cell targeting of semiconductor CdSe/ZnS nanocrystals with phytochelatin-related peptides. J Am Chem Soc 126:6115–6123.

Rasnik I, McKinney SA, Ha T (2006) Nonblinking and long-lasting single-molecule fluorescence imaging. Nat Methods 3:891–893.

Rasse TM, Fouquet W, Schmid A, Kittle RJ, Mertel S, Sigrist CB, Schmidt M, Guzman A, Merino C, Qin G, Quentin C, Madeo FF, Heckmann M, Sigrist SJ (2005) Glutamate receptor dynamics organizing synapse formation in vivo. Nat Neurosci 8:898–905.

Schmidt T, Schutz GJ, Baumgartner W, Gruber HJ, Schindler H (1995) Characterization of photophysics and mobility of single molecules in a fluid lipid membrane. J Phys Chem 99:17662–17668.

Sekine-Aizawa Y, Huganir RL (2004) Imaging of receptor trafficking by using alpha-bungarotoxin-binding-site-tagged receptors. Proc Natl Acad Sci USA 101:17114–17119.

Serge A, Fourgeaud L, Hemar A, Choquet D (2002) Receptor activation and homer differentially control the lateral mobility of metabotropic glutamate receptor 5 in the neuronal membrane. J Neurosci 22:3910–3920.

Sharma K, Fong DK, Craig AM (2006) Postsynaptic protein mobility in dendritic spines: long-term regulation by synaptic NMDA receptor activation. Mol Cell Neurosci 31:702–712.

Svoboda K, Yasuda R (2006) Principles of two-photon excitation microscopy and its applications to neuroscience. Neuron 50:823–839.

Tardin C, Cognet L, Bats C, Lounis B, Choquet D (2003) Direct imaging of lateral movements of AMPA receptors inside synapses. EMBO J 22:4656–4665.

Thomas P, Mortensen M, Hosie AM, Smart TG (2005) Dynamic mobility of functional GABAA receptors at inhibitory synapses. Nat Neurosci 8:889–897.

Tovar KR, Westbrook GL (2002) Mobile NMDA receptors at hippocampal synapses. Neuron 34:255–264.

SUPPLEMENTARY BOX 2

1. Schematic guideline for single molecule/QDot trajectory construction

For trajectory contruction, SD and QDots are first identified through their spatial intensity distribution. The most straightforward method to retrieve the position of the objects is to perform two dimensional fitting the full intensity distribution of each spot by a Gaussian approximating the true point spread function of the microscope. This approach is the most sensitive and well suited for dim molecules such as dye molecules. The main drawback is that it is computer time consuming. For brighter emitters like QDots, less sensitive algorithms can be used to reduce the computation time. We present in the following such a fast algorithm that relies on wavelet transforms that filters the image frames and identifies the QDots through their morphology alone and not their absolute intensity signals. Once the positions of the objects are determined, the reconstruction of the trajectories has to be performed. We present two strategies, the Vogel algorithm for SD which performs a correlation analysis between the positions of the SD found in *consecutive* images and the Multidimensional Image Analysis package for QDots which is based on a *multi-frame* object correspondence problem looking globally for the minimal energy of all possible trajectories using the simulated annealing algorithm.

2. Trajectory construction of fluorescent dye molecule: the Vogel algorithm

Once the fluorescent spots are detected in each image, the two-dimensional trajectories of single molecules in the plane of focus are constructed by correlation analysis between consecutive images using a Vogel algorithm (Schmidt et al., 1995). This method connects simultaneously several pairs of spots detected in two successive images by minimizing the deviation of the mean diffusion constant of the connected spots with respect to a given diffusion constant, Dpred (Fig. 1, 2). In other words, the trajectory of one molecule will add one point in an image if there is a fluorescent spot within a statistically relevant distance from the position of the previous point. If there is no connection possible, the trajectory is finished (Tardin et al., 2003; Groc et al., 2004; Groc et al., 2006). The termination of the trajectories can reflect the photobleaching of the dye or the diffusion perpendicular to the observation plane what makes the molecule to exit the detection volume. For this reason, new molecules not present at the beginning of the recording can appear during the image sequence. Dpred is determined performing a preparative analysis varying its value (Fig. 1) and selecting the one that allows the better connections between spots. By varying Dpred in the analysis, it is possible to accurately retrieve the molecule trajectories and to check the validity of the experimental labelling conditions. Indeed, when a too small value of Dpred is used in the program, only portion of trajectories where molecule performed small displacements are retrieved. In this case, only very short trajectories are obtained with a mean diffusion constant equal to Dpred (Fig. 2). On the contrary, using a very large

Dpred,, the Vogel algorithm will privilege the connection between spots that belong to different molecules, giving aberrant trajectories and high measured diffusion value (Dmeas). Between those two cases, trajectory construction should lead to a constant Dmeas, independent the choice of Dpred as evidenced by the curve plateau in Fig. 2. This plateau should be obtained for each experiment and when this is not the case the labelling density of molecules is too high to retrieve accurately the trajectories and the analysis stops.

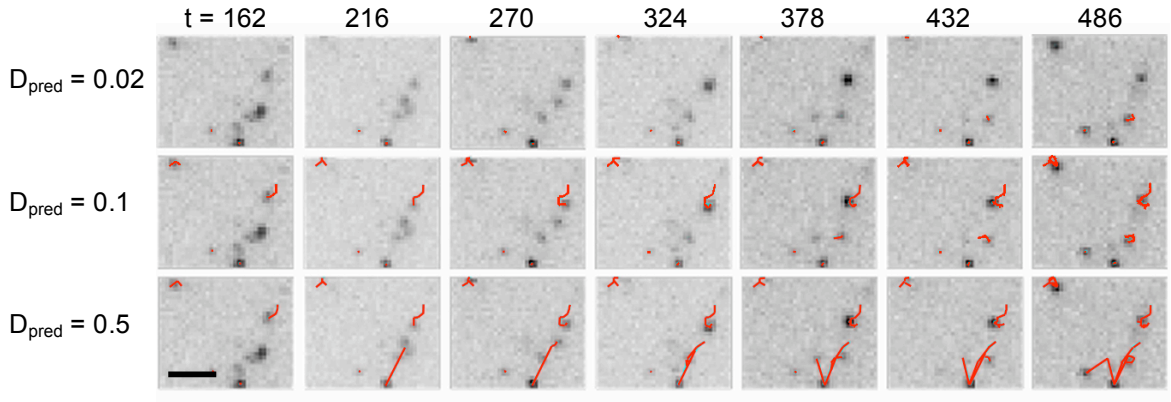

Figure 1. Series of image frames showing the trajectory reconstruction as a function of a given diffusion constant (D_{pred}). Diffusion unit is in $\mu m^2/s$; time unit (t) is in ms; scale bar = 2 µm. The image series does not start at time 0 in order to exemplify the effect of change in D_{pred} on already existing trajectories.

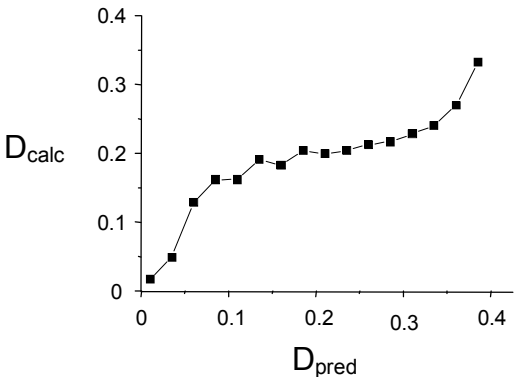

Figure 2. Calculated diffusion constant (D_{calc}) retrieved as a function of D_{pred}. Diffusion unit is in $\mu m^2/s$.

3. Tracking of QDots: the multi-dimensional image (MIA) analysis

As already mentioned, the superior brightness and photostability of QDots make them particularly attractive for wider (thousands of square-micrometers) and longer (minutes) recording fields than SDs (typically up to 1000µm² and few seconds) (Dahan et al., 2003; Groc et al., 2004; Groc et al., 2006;

Bats et al., 2007). This allows the simultaneous minutes long recording of many QDots but at the obvious price of increased complexity in data analysis. Due to their brightness the use of a faster detection algorithm than Gaussian fitting of the signals was possible to reduce the computation time of large fields recordings. Detection and tracking of QDots are thus performed with a dedicated multi-dimensional image analysis software described in Supplementary Methods. This software has been developed at the Imaging Facility at the Curie Institute as user-friendly software provided as a plug-in for Metamorph (Molecular Device) (http://www.curie.fr). The graphical interface is written in Visual Basic whereas the image analysis routines are based on speed-optimized C^{++} codes. Note that this algorithm which is highly appropriate for QDots is however less sensitive than Gaussian fitting and could not be used to analyse dimmer objects such as fluorescent dye molecules.

3.1 Multidimensional Image Analysis software description

The algorithm retrieves the fluorescence spot positions based on their morphology instead of the 2D fitting of the signals. Schematically, segmentation of individual bright objects was performed using a dyadic undecimated fast wavelet transform, and trajectory reconstruction was achieved by minimizing association costs between successive objects using a simulated annealing algorithm.

3.2. Object segmentation

Region based segmentation is used to detect bright spots from the backgrounds. The initial image is decomposed into a set of wavelet maps that embed different level of details, from the finer to the coaster. The implemented wavelet transform is called “à trous” algorithm (Shensa, 1992). It is an undecimated (i.e. the coefficient number of each wavelet map is equal to the pixel number of the initial image) and dyadic (i.e. the size of the analyzing wavelet doubles between two consecutive maps) algorithm. The implemented wavelets (third order B-Spline) (Unser and Aldroubi, 1992) are isotropic, thus the detection is more adapted to the segmentation of isotropic objects like in the images of QDots. Strong advantages of the “à trous” algorithm are its very fast computation (according to the fast wavelet transform) and its good precision (the undecimated property leads to redundant information) (Starck et al., 1998). Using the graphical interface, the user needs to choose first, the wavelet map(s) where the objects of interests are well defined. Secondly, each map is segmented using user defined threshold value which allows the successful extraction of the objects from the background, based on the correct morphology of the extracted objects with comparison of the point spread function of the microscope. As the threshold is operated in the wavelet maps, the heterogeneous background does not affect the spot detection. The segmentation is applied on all the frames with the same parameters (maps and threshold values).

3.2.1. Object tracking

The tracking procedure is resolved as a multi-frame object correspondence problem. For this purpose,

we use the simulated annealing algorithm for its flexibility for feature correspondence and its ability to give results in a very short time (Racine et al., 2006).

3.2.2 Correspondence problem

This approach takes into account events like “birth” and “death”. We use an energy minimization-based approach for object trajectory reconstruction in 2D+t and 3D+t images of cellular and sub-cellular structures acquired by video-microscopy.

For the correspondence problem, an object is allowed to appear and disappear as well as to enter and leave the field. This is motivated by the image resolution and signal to noise ratio, often leading to weak spots impossible to precisely segment. Moreover, the blinking of the QDots, leads to fluorescent object appearance and disappearance which is consistent with birth and death events. We solve the correspondence problem using the simulated annealing algorithm for its flexibility to modulate constraints according to physical situations, for its rapidity since the number of variables used in the energy calculation is low, and finally because it does not require any particular track initialization.

We use several features to provide a reliable representation for object correspondence. Each object is described by its centre of mass *c(O)* where *O* denotes an object, its average intensity *I(O)* and its sum of intensity *S(O)*. These features encode a global description of how the object appears. To deal with death and birth events, features of a empty object, called dummy object *ø* are also considered, except that its centre of mass is defined by *I(ø)=0* and *S(ø)=0*.

A connection corresponds to the matching hypothesis between two objects detected in two successive frames. We distinguish tree different events as described in Fig. 3A. In the case of a continuation event, the two objects from two successive frames are connected. In the case of a death (resp. birth) event, an object is connected in the future (resp. past) to a dummy object. The connections must be coherent, meaning that each object is connected in the future (resp. past) either to an object of the next (resp. previous) frame or a dummy object. The set of connections of all the objects of all the frames is called a “coherent solution” (Sol) of the assignment problem.

3.3. Energy functions

The global energy J(Sol) associated to a coherent solution *Sol* is defined as the sum of the individual energies of all events for all times. The energy of any event can be written as *E(A, B)* where *A* is an object of the frame *i* and *B* of the frame *i+1*. Depending on the event type, *A* or *B* can be a dummy object. The energy *E(A, B)* is defined by:

$E(A, B) = n\ I$

Where $E_c(A,B) = 1$ for death and birth events and $E_c(A,B) = \left\| c(A) - c(B) \right\|_2^2 / \sigma_c^2$ otherwise;

$E_I(A,B) = (I(A) - I(B))^2 / \sigma_I^2$

$E_S(A,B) = (S(A) - S(B))^2 / \sigma_S^2$

n defines the number of objects implicated in the event, $n = 1$ for birth and death events and $n = 2$ for a continuation event. $\|.\|_2$ represents the Euclidean norm. σ_c^2, σ_I^2 and σ_S^2 are scale parameters describing the standard deviations associated to each feature. In the case of birth (resp. death) events, the localization energy $E_c(\emptyset,B)$ (resp. $E_c(A,\emptyset)$) is set to 1 in order to consider the dummy object $\emptyset$ at a distance σ_c from the object B (resp. A). The energy definition allows to handle the blinking of the fluorescent molecules as well as missed detections and false alarms due to segmentation errors. A birth event followed by a death event will be considered as a false alarm, while a death event followed by a birth event will be considered as a missed detection. In this last case, the object trajectory will be split.

3.4. Simulated Annealing Algorithm

Thus far, we are able to compute the energy associated to a coherent solution. The objective of the algorithm is to find the solution *Sol** that best minimizes the global energy. Scale parameters σ_c^2, σ_I^2 and σ_S^2 are used to control the standard deviations associated to each feature. These values change according to the different parameters of the moving objects and the acquisition frame rate. They can be set by the user for a particular experiment or guessed by resolving the object tracking using a simple algorithm like the nearest neighbor. A first solution Sol^0 is initialized such as there is no continuation event. We use the simulated annealing algorithm (Press et al., 1992) to reach the optimal solution starting from the initial solution Sol^0 while decreasing the temperature T. At the k^{th} iteration, a local change in the solution Sol^k is tested and eventually kept. All possible local changes are summarized in Fig. 3B. We consider that the convergence is reached when no more change is allowed, then the optimal solution *Sol** is obtained.

The obtained trajectories are exported as a hyper text file, where the statistical information is stored (Fig. 4). This file can be loaded in any software for further exploitation of the trajectories, as shown in the Fig. 5. The segmented objects can also be exported as a time series of images where each segmented object has a unique tag over the time. The user can do a visual inspection of the results to validate them.

3.5. Taking into account the blinking of quantum dots: connection of subtrajectories.

Different approaches can be used to take into account blinking in trajectory reconstructions (Bonneau et al., 2005; Bachir et al., 2006). In most cases, a simple method can be used connecting iteratively trajectories already constructed during the non-blinking states. To allow the connection, we set criteria in time (amount of images without signal) and space (the distance roamed during blinking). More

precisely, in a given iteration, the last position of the molecule of the first trajectory is connected to the first position of the closest following trajectory, only if it is within a time and a spatial limit. The same procedure is used for all trajectories and repeated iteratively until no connexions are allowed. The QDots observed in D blinks over approximately few seconds as can be seen in the plot of its intensity versus time. After reconnection, the movements are successfully tracked over the whole observation time. Additional constraints can be added into the reconnection analysis. For instance, blinking period that are longer than a determined period (e.g. few seconds) are considered as ending/starting time point for trajectories.

A

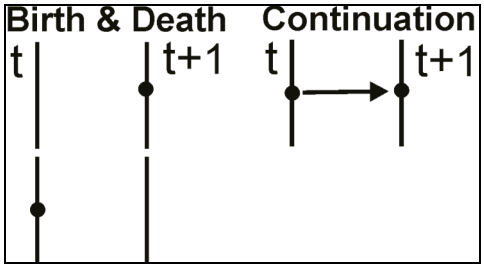

B

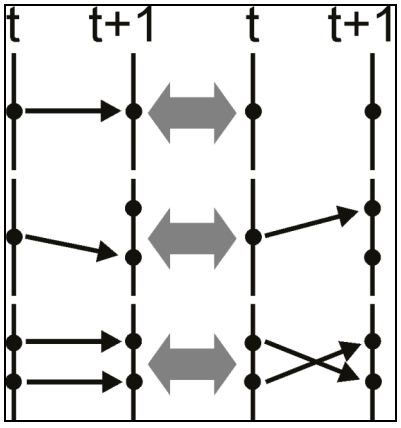

Figure 3. ***A*****,** Representation of the selected event types. ***B***, Different changes of configuration operated during the optimization algorithm. The grey double arrows indicates that the left configuration can be replace be the right one.

Tracking report and statistics

This file has been generated by "C:_DLL\tracking.exe" from MIA software
The current date is 02/14/07 (mm/dd/yy) and the current time is 16:51:14
53 tracked structures found with a minimum of 2 times long
The standard variation of the intensity sum is 369.486337
The standard variation of the intensity average is 16.811171
The standard variation of the distance is 0.595451

Structure 1 *Color 1*

The structure 1 (color 1) appears at the time 0

Duration	First Time	Last Time	Total distance	time scale MSD
100	0	99	1.64	0.89

Time	0	1	2	3	4	5	6	7	8	9	10
Pos X	35.69	35.60	35.59	35.60	35.65	35.64	35.62	35.64	35.88	35.93	35.
Pos Y	26.52	26.22	26.24	26.29	26.22	26.22	26.19	26.26	26.73	26.99	26.
Speed	0.00	0.31	0.03	0.05	0.09	0.01	0.03	0.07	0.53	0.27	0.1
Surface	18	16	16	17	17	17	15	16	19	21	20
IntensityAverage	184.91	184.71	190.05	188.36	179.66	187.37	170.00	196.43	171.66	165.84	15
IntensitySum	3328.47	2955.39	3040.85	3202.11	3054.26	3185.34	2549.97	3142.92	3261.52	3482.72	30

The structure 1 (color 1) disappears at the time 99
Top

Structure 2 *Color 2*

The structure 2 (color 2) appears at the time 0

Duration	First Time	Last Time	Total distance	time scale MSD
16	0	15	3.43	0.92

Time	0	1	2	3	4	5	6	7	8	9	10
Pos X	62.40	62.49	62.75	64.92	65.72	64.94	65.64	66.30	66.43	66.76	66.
Pos Y	14.11	14.03	14.06	13.64	13.61	13.47	13.63	13.64	13.63	13.55	13.
Speed	0.00	0.12	0.27	2.21	0.80	0.79	0.71	0.67	0.13	0.34	0.0
Surface	15	16	16	26	23	20	18	21	23	18	17
IntensityAverage	136.24	133.68	125.23	112.56	126.17	138.25	161.38	149.52	122.64	149.60	16
IntensitySum	2043.56	2138.93	2003.60	2926.54	2901.93	2765.02	2904.79	3139.96	2820.83	2692.85	27

The structure 2 (color 2) disappears at the time 15
Top

Figure 4. HTML file generated by the MIA software representing 2 objects over the time.

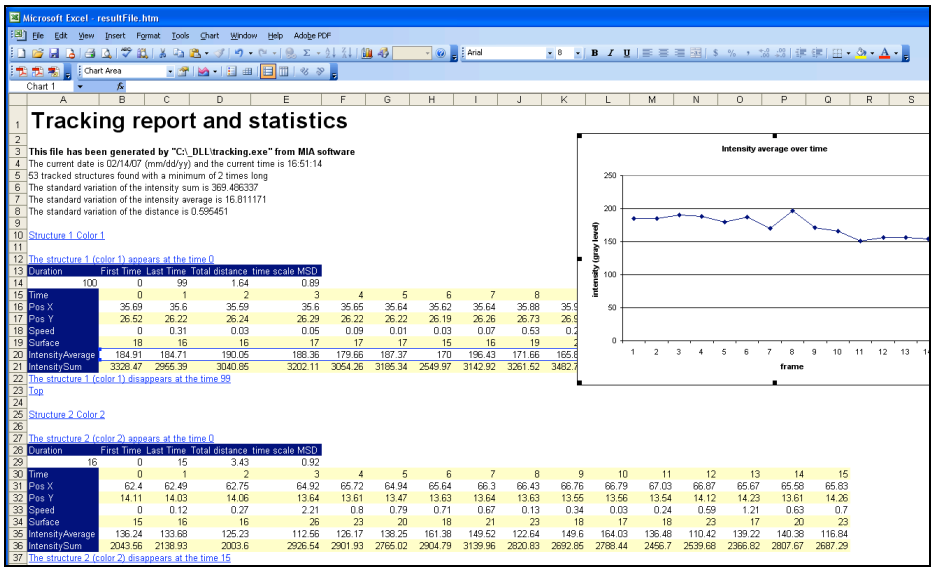

Figure 5. HTML file loaded in Microsoft Excel to be analyzed.

References

Bachir A, Durisic N, Grutter P, Wiseman P (2006) Characterization of blinking dynamics in quantum dot ensembles using image correlation spectroscopy. J Appl Phys 99:064503.

Bats C, Groc L, Choquet D (2007) The interaction between Stargazin and PSD-95 regulates AMPA receptor surface trafficking. Neuron 53:719-734.

Bonneau S, Dahan M, Cohen L (2005) Single quantum dot tracking based on perceptual grouping using minimal paths in a spation temporal volume. IEEE Transactions in Image Processing 14:1384-1395.

Dahan M, Levi S, Luccardini C, Rostaing P, Riveau B, Triller A (2003) Diffusion dynamics of glycine receptors revealed by single-quantum dot tracking. Science 302:442-445.

Groc L, Heine M, Cognet L, Brickley K, Stephenson FA, Lounis B, Choquet D (2004) Differential activity-dependent regulation of the lateral mobilities of AMPA and NMDA receptors. Nat Neurosci 7:695-696.

Groc L, Heine M, Cousins SL, Stephenson FA, Lounis B, Cognet L, Choquet D (2006) NMDA receptor surface mobility depends on NR2A-2B subunits. Proc Natl Acad Sci U S A 103:18769-18774.

Press WH, Teukolsky SA, Vetterling WT, Flannery BP (1992) Numerical recipes in C. Cambridge University Press, USA.

Racine V, Hertzog A, Jouanneau J, Salamero J, Kervrann C, Sibarita J-B (2006) Multiple-target tracking of 3D fluorescent objects based on simulated annealing. IEEE International Symposium on Biomedical Imaging:1020-1023.

Schmidt T, Schutz GJ, Baumgartner W, Gruber HJ, Schindler H (1995) Characterization of photophysics and mobility of single molecules in a fluid lipd membrane. J Phys Chem 99:17662-17668.

Shensa MJ (1992) The discrete wavelet transform: Wedding the A trous and mallat algorithms. IEEE Transactions on Signal Processing 40:2464.

Starck J-L, Murtagh F, Bijaoui A (1998) Image processing and data analysis: the multiscale approach. Cambridge University Press, USA.

Tardin C, Cognet L, Bats C, Lounis B, Choquet D (2003) Direct imaging of lateral movements of AMPA receptors inside synapses. Embo J 22:4656-4665.

Unser M, Aldroubi A (1992) Polynomial splines and wavelets: a signal processing perspective. Academic Press Professional, Inc, San Diego, CA, USA.

Supplementary BOX 1

Single dye identification

In each image of the recorded sequence, the single molecules appear as diffraction-limited bright spots, as shown in Fig. 1. For image analysis, single dye identification is performed by a custom made program (Matlab) (Tardin et al., 2003; Groc et al., 2004; Groc et al., 2006). The program obtains the positions and the errors in positioning for each fluorescent signal (spots) fitting a two-dimensional Gaussian to the intensity (I) patterns of the spot (Schmidt et al., 1996a; Cheezum et al., 2001):

$I(x,y) = A_n \exp(-((x-x_n)^2 + (y-y_n)^2)/2\,\sigma_n^2)$

where n is the image number; A_n is the amplitude of the Gaussian (given as a greyscale value in the images); σ_n is related to the full width at half maximum of the pattern by FWHM = $2(2 \ln 2)1/2\sigma_n$. Given by the point-spread of our set-up, FWHM = 360 ± 40 nm. The parameters x_n and y_n give the central positions of the spot. The errors in the four parameters A_n, x_n, y_n and σ_n vary for each analysed spot because the fitting accuracy depends on the signal-to-noise ratio. The errors in x_n and y_n represent the positioning accuracy and are typically well below the optical resolution limit, typically 50 nm for cyanine dyes (Schmidt et al., 1996b; Tardin et al., 2003). The width of the fitted curve and the difference of intensity are compared to cut-off parameters.

Only spots bearing the two characteristic signatures of single molecules, i.e. one-step photobleaching and diffraction limited signal, are retained for analysis (Fig. 1). This is confirmed by the narrow and unimodal shape of the frequency distribution of the number of counts originating from individual spots detected in an image (Fig. 2) (Tardin et al., 2003). In our example with Cy5, the maximum of the distribution was 630 counts/30 ms, n = 3078). The peak of the probability function corresponding to the background in condition of the experiments is 28 counts per 30 ms which translates in a signal-to-noise greater than 20. The corresponding theoretical pointing accuracy was 45 nm. This was further confirmed experimentally by either analysing the statistical errors found in the determination of x_n and y_n for cyanines dried on a glass coverslip or from the value found at time zero in the Mean Square Displacement (MSD, “area explored over time”) analysis of moving molecules.

More precisely, for a trajectory of N data points (coordinates x(t), y(t) at times t = 0 to N* Δt with Δt = 30 ms), the MSD for time intervals $\tau = n\Delta t$ is calculated using the formulae:

$$\sum_{i=1}^{N-n} \frac{\left[x((i+n)*\Delta t) - x(i*\Delta t)\right]^2 + \left[y((i+n)*\Delta t) - y(i*\Delta t)\right]^2}{N-n}$$

For the time interval $\tau = n\Delta t$, the MSD and its error bar are thus calculated on N-n points. The typical pointing accuracy which corresponds to the square root of the MSD at τ = 0 is typically 45 nm for SD and 30 nm for QDots.

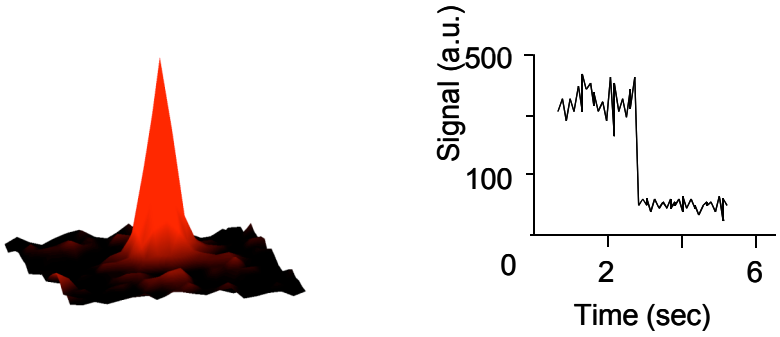

Figure 1. The two characteristic signatures of single molecules: diffraction limited signal (left panel) and one-step photobleaching (rigth panel).

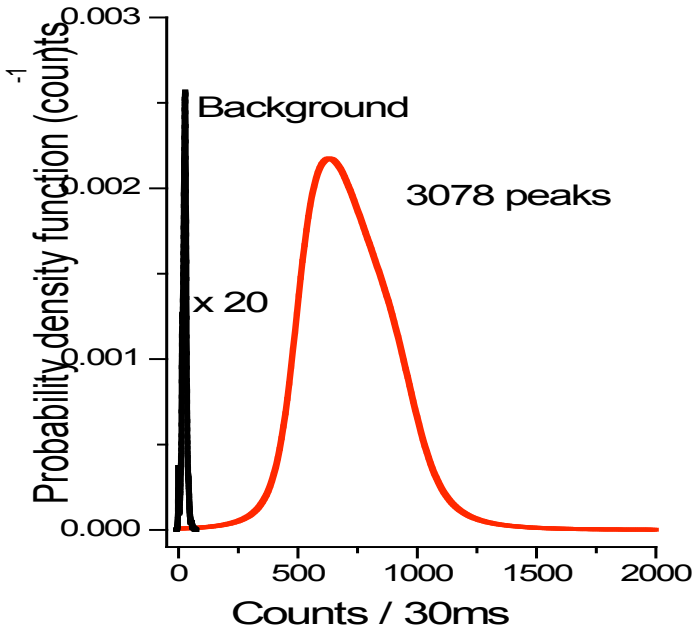

Figure 2. Probability density function of the intensities retrived from the 2D Gaussian fit of 3078 fluorescent spots (red) recorded on live neurons stained with Cy5-labelled anti-GluR2 antibodies. The black curve corresponds to the probability distributiqon of the background signals recorded on spots of the same area.

References

Cheezum M, Walker W, Guilford W (2001) Quantitative comparison of algorithms for tracking single fluorescent particles. Biophys J 81:2378-2388.

Groc L, Heine M, Cognet L, Brickley K, Stephenson FA, Lounis B, Choquet D (2004) Differential activity-dependent regulation of the lateral mobilities of AMPA and NMDA receptors. Nat Neurosci 7:695-696.

Groc L, Heine M, Cousins SL, Stephenson FA, Lounis B, Cognet L, Choquet D (2006) NMDA receptor surface mobility depends on NR2A-2B subunits. Proc Natl Acad Sci U S A 103:18769-18774.

Schmidt T, Schuetz GJ, Baumgartner W, Gruber HJ, Schindler H (1996a) Imaging of single molecule diffusion. Proc Natl Acad Sci U S A 93:2926-2929.

Schmidt T, Schuetz GJ, Baumgartner W, Gruber HJ, Schindler H (1996b) Imaging of single molecule diffusion. ProcNatlAcadSciUSA 93(7):2926-2929.

Tardin C, Cognet L, Bats C, Lounis B, Choquet D (2003) Direct imaging of lateral movements of AMPA receptors inside synapses. Embo J 22:4656-4665.

SUPPLEMENTARY BOX 3

The surface diffusion of both endogenous and transfected recombinant glutamatergic subunits were compared using data collected from published (Groc et al., 2006; Bats et al., 2007) and unpublished studies from our laboratory. The surface diffusion of two types of recombinant GluR2 subunits (BBS-GFP-GluR2 in the present report and a GFP-GluR2 construct) were compared with endogenous GluR2 in hippocampal cultured neurons (10-20 days *in vitro*). GFP was inserted in the extracellular domain of both recombinant subunits, which were transfected into neurons using lipofectamine 2000 (Invitrogen). Because neurons transfected with recombinant GluR2 subunits also expressed endogenous subunits, recombinant GluR2 subunits were tracked using anti-GFP antibody (24-36 h after transfection). As shown below, the percent of immobile endogenous and recombinant GluR2-containing AMPARs are comparable. The same conclusion can be drawn from the comparison of the instantaneous diffusion coefficients (see below, rigth panel). These data indicate that the surface trafficking of endogenous and recombinant GluR2 subunits is rather similar.

On the opposite, the surface trafficking of NR2B subunits from either naive or NR2B-transfected neurons provide different results. A pH-sensitive GFP (super ecliptic pHluorin) was inserted in the extracellular domain of NR2B subunits and hippocampal cultured neurons (10-15 days *in vitro*) were transfected with the recombinant subunits using lipofectamine 2000 (as for the GluR2 subunits above) (Groc et al., 2006). As previously described (Groc et al., 2006), the endogenous NR2B subunits were tracked using an anti NR2B N-terminal domain antibody whereas recombinant pHluorin GFP-NR2B subunits were tracked using anti-GFP antibody (same as one used above for GFP-GluR2 subunits). When examined 24-36 h after transfection, overexpression of NR2B subunits induces a right shift of the cumulative distribution of NR2B diffusion coefficient (see panels below). These results are consistent with an increased surface trafficking of recombinant NR2B subunits.

All together, these results highlight 1) a difference in the effect of overexpression between two subunit types (GluR2 versus NR2B), and 2) a difference between endogenous and recombinant subunits (only for NR2B). These results are only indicative for these specific experimental designs and may vary with different transfection method, subunit types, or neuronal stages. Such comparison strongly suggests that appropriate control (e.g. comparison between endogenous and recombinant subunit surface trafficking and content) is required for each study.

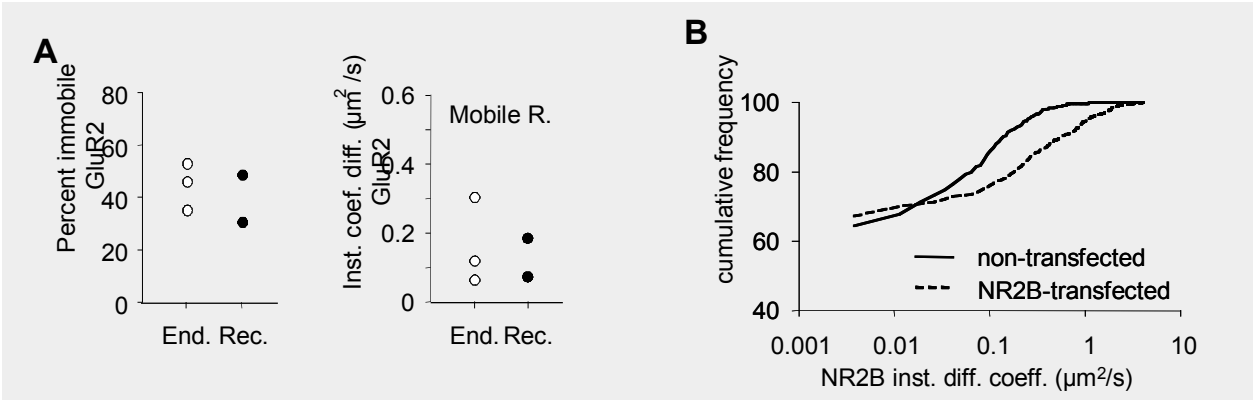

Comparison of surface trafficking between endogenous and recombinant glutamatergic subunits. ***A***, The percent of immobile receptor (left panel) as well as the diffusion coefficient of mobile receptors were compared between endogenous (End.) and recombinant (Rec.) GluR2 subunits. Each dot represents an average value obtained from independent study. ***B***, Cumulative distributions of the surface diffusion of NR2B subunits from untransfected and NR2B-transfected hippocampal cultured neurons. Note the significant rigth shift of the NR2B-transfected distribution ($P < 0.001$, Kolmogorov-Smirnov test).